

# Chiral Majorana edge states in HgTe quantum wells

L. Weithofer<sup>1</sup>, P. Recher<sup>1</sup>

<sup>1</sup> Institute for Mathematical Physics, TU Braunschweig,  
38106 Braunschweig, Germany

E-mail: [p.recher@tu-bs.de](mailto:p.recher@tu-bs.de)

**Abstract.** HgTe-based quantum wells (QWs) recently attracted a lot of attention for the realization of a two-dimensional topological insulator with protected helical edge states. Another class of topological systems are topological superconductors (TSCs) with Majorana edge states. In this paper, we show how proximity induced s-wave superconductivity in the bulk of HgTe-QWs and in the presence of a Zeeman field can exhibit a TSC with chiral Majorana edge states. We calculate the topological invariants and the corresponding Majorana edge states explicitly within a four-band model accounting for inversion symmetry breaking terms due to Rashba spin-orbit coupling and bulk inversion asymmetry present in these QWs.

PACS numbers: 74.25, 71.10, 73.20, 73.43, 73.63

Submitted to: *New J. Phys.*

## 1. Introduction

The search for Majorana quasiparticles in condensed matter systems is a subject of great fundamental and practical interest. Majorana quasiparticles have been recently proposed to exist in various systems which typically combine strong spin-orbit coupling (SOC), the proximity to an s-wave superconductor and magnetic elements [1, 2, 3, 4].

In particular, Majorana bound states (MBS) have been proposed to emerge in vortex cores on the surface of strong three-dimensional (3D) topological insulators (TIs) [5] or at the edges of two-dimensional TIs when brought to the proximity of an s-wave superconductor and a magnet [6, 7]. Characteristic features of Majorana fermions have also been predicted in spin-orbit coupled two-dimensional semiconductors [8, 9] and one-dimensional spin-orbit coupled semiconductor nanowires [10], and very recent experiments show signatures of MBS which are currently being scrutinized [11, 12, 13]. In these semiconductor systems, time-reversal symmetry is broken by a Zeeman splitting which, in addition to the proximity of an s-wave superconductor, is necessary to induce a TSC. In such systems, a large SOC is desirable as the vulnerability of the energy gap to disorder typically depends on the size of SOC [14, 15]. If the Zeeman splitting is induced by external magnetic fields, low field strengths and therefore small orbital effects are beneficial for the superconducting correlations, which favors semiconducting materials with large effective g-factors.

In this work we show that a doped HgTe-QW can implement a TSC, when s-wave superconductivity and a Zeeman-field is induced in the QW. In order to describe the HgTe-QW, we use the four-band BHZ model [16, 17, 18] valid near the transition between the inverted and non-inverted regime. In the inverted regime and in the absence of superconductivity and a Zeeman gap, the well-known helical edge states appear in the spectral bulk gap [16, 19, 20]. Importantly, HgTe-QWs are intrinsically subjected to inversion symmetry breaking SOC due to bulk inversion asymmetry (BIA) [18, 21] which breaks the Kramer's spin-degeneracy. We show that BIA-SOC alone is sufficient to induce a TSC when superconductivity and a Zeeman gap are added. However, tunable (extrinsic) inversion symmetry breaking terms provided by Rashba-SOC can be added as well.

It is known that HgTe-QWs are characterized by a very large Rashba-SOC [22], which can be one order of magnitude larger compared to other III-V compound semiconductors [22, 23]. In [22], Rashba-splittings in inverted HgTe-QWs as large as 30 meV were reported. In addition, the effective Zeeman gap in a perpendicular magnetic field was recently calculated and measured in zero gap samples to be consistent with an effective g-factor  $g^* \sim 55.5$  [24]. This shows that HgTe-based QWs could be a feasible candidate for a proximity induced TSC.

In addition to a potentially feasible implementation of already existing ideas, we show that the combination of BIA and Rashba SOC provides an interesting handle on the topological properties of the TSC. In particular, we show that (consistent with topological invariants) the chirality of Majorana edge states can be reversed by changing

the relative strength of the two SOC terms.

In contrast to the proposal of using 1D helical edge states as a platform for MBS [5], we would like to point out in this work the possibility of switching between chiral (Majorana) and the well-known helical edge states on the same one-dimensional boundary of a HgTe-QW.

The paper is organized as follows. In section 2 we introduce the setup and the relevant model Hamiltonian. Subsequently, we describe the bulk properties of the system, emphasizing the topologically non-trivial and trivial phases of the system in section 3. In section 4, we solve the chiral Majorana edge states at a domain wall between topologically non-trivial and trivial phases and calculate the group velocity along the edge. Finally, we compare the chiral Majorana edge states that emerge when the system is in a TSC phase to the helical edge states that emerge in a TI phase in section 5.

## 2. The Model

We consider a doped HgTe-QW in the  $xy$ -plane in contact to an s-wave superconductor, as sketched in figure 1. There are two inversion $\ddagger$ -asymmetry induced SOC effects: Firstly, BIA-induced SOC is intrinsically present as a consequence of the zinc blende structure of the underlying crystal. Secondly, so-called Rashba-SOC arises when an external electric field is applied in  $z$ -direction. In addition, a Zeeman field is present in  $z$ -direction which can be induced by the proximity to a ferromagnetic insulator (via spin-exchange interaction), or intrinsically by using Mn-doped ( $\text{Hg}_{1-y}\text{Mn}_y\text{Te}$ ) QWs and a small external magnetic field polarising the Mn-spins [25]. Although a magnetic field induces also an orbital effect not taken into account here, we note that the vector potential of a perpendicular magnetic field induces an additional Zeeman splitting between the Kramer's spins with an effective giant  $g$ -factor of  $g^* \sim 55.5$  [24] so that only small external magnetic fields below 1T would be needed.

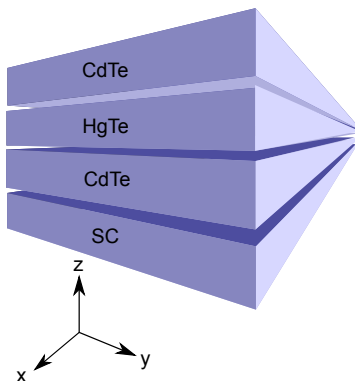


**Figure 1.** HgTe-QW in proximity to an s-wave bulk superconductor (SC).

$\ddagger$  i. e.  $(x, y, z) \rightarrow -(x, y, z)$

The resulting QW system is described in terms of the BHZ model [16], complemented with extra terms accounting for BIA [18], Rashba [17], Zeeman field [18, 25], and the proximity to an s-wave superconductor [26]. The Hamiltonian can be written in the basis order  $\psi_{E1+}, \psi_{H1+}, \psi_{E1-}, \psi_{H1-}, \psi_{E1-}^\dagger, \psi_{H1-}^\dagger, -\psi_{E1+}^\dagger, -\psi_{H1+}^\dagger$  in terms of products of the Pauli matrices  $\underline{s}, \underline{\sigma}, \underline{\tau}$  and the identity matrix, where  $\underline{s}$  acts in pseudospin ( $E1, H1$ )-space,  $\underline{\sigma}$  acts in Kramer's spin space $\S$  and  $\underline{\tau}$  acts in electron-hole space. The extended BHZ-model Hamiltonian reads

$$\begin{aligned} H = & \left( \epsilon(\hat{k}^2) + M(\hat{k}^2)s_z + A\hat{k}_x s_x \sigma_z - A\hat{k}_y s_y \right) \tau_z \\ & + h(\cos 2\theta \sigma_y + \sin 2\theta \sigma_x) s_y \tau_z \\ & + R_0 \frac{(s_z + 1)}{2} \left( \hat{k}_x \sigma_y - \hat{k}_y \sigma_x \right) \tau_z \\ & + (B_+ + B_- s_z) \sigma_z + (\Delta_+ + \Delta_- s_z) \tau_x. \end{aligned} \quad (1)$$

with

$$\epsilon(\hat{k}^2) = C - D(\hat{k}_x^2 + \hat{k}_y^2), \quad M(\hat{k}^2) = M - B(\hat{k}_x^2 + \hat{k}_y^2) \quad (2)$$

$$B_\pm = (B_E \pm B_H)/2, \quad \Delta_\pm = (\Delta_E \pm \Delta_H)/2. \quad (3)$$

Here,  $\hat{k}_x$  and  $\hat{k}_y$  denote the differential operators  $-i\partial_x$  and  $-i\partial_y$ .

The material parameters  $A, B, D, M$  depend on the geometry of the QW. In particular, the mass parameter  $M$  is tunable by the QW thickness. The BHZ-model was successfully used to explain experimental transport data for mass-parameters in the range  $-24 \text{ meV} \leq M \leq 10 \text{ meV}$  [27]. The parameter  $C$  defines the doping of the QW (tunable by top and/or bottom gates).

The two additional SOC terms have coefficients denoted by  $h$  for the BIA term and  $R_0$  for the linear Rashba term $\parallel$ . As the BIA term is not invariant under rotation in the  $xy$  plane, the angle  $\theta$  is introduced to describe the angle between the  $x$ -axis and the [100] crystal direction.

The pairing terms  $\Delta_E$  and  $\Delta_H$  describe the effect of the s-wave superconductor on the  $E1$  and  $H1$  bands. We neglect a possible off-diagonal proximity coupling between  $E1$  and  $H1$  bands and without loss of generality assume that the pairing terms  $\Delta_E$  and  $\Delta_H$  in (1) are real [26].

Typical values of the above mentioned parameters are presented in table 1. As Zeeman energy of the  $E1$  and  $H1$  bands, we use  $B_E = 1.3 \text{ meV}$  and  $B_H = -0.07 \text{ meV}$ , respectively. In addition,  $\mathcal{E} = 3 \text{ mV/nm}$  is assumed as an effective electric field invoking the Rashba-SOC. Unless stated otherwise, we also use a doping parameter of  $C = 7.8 \text{ meV}$  and  $\theta = 0$ , as well as  $\Delta_E = 0.5 \text{ meV}$  and  $\Delta_H = 0.5 \text{ meV}$  for the superconducting proximity terms $\P$ .

$\S$  The quantum number that transforms under time reversal. The electron spin is not a good quantum number in the presence of spin-orbit interactions.

$\parallel$  Rashba terms of higher order in  $k$  are neglected.

$\P$  In reality,  $\Delta_E$  and  $\Delta_H$  will not be exactly equal, however, in our parameter regime  $C \approx -M$  (see below), the dominant contribution will come from  $\Delta_E$ .

| $A$        | $B$                     | $D$                     | $M$       | $h_{\text{BIA}}$ | $R_0/(e\mathcal{E})$  |
|------------|-------------------------|-------------------------|-----------|------------------|-----------------------|
| 3.645 eV Å | -68.6 eV Å <sup>2</sup> | -51.2 eV Å <sup>2</sup> | -0.008 eV | 0.0016 eV        | -15.6 nm <sup>2</sup> |

**Table 1.** Typical values for the parameters of the inverted HgTe-QW as taken from [18, 17].

### 3. Bulk Physics

#### *BIA-SOC is sufficient*

Firstly, we show that BIA-SOC is sufficient in order to overcome the ‘fermion doubling problem’ [3] by freezing out half the degrees of freedom (unless  $k = 0$ ), which otherwise would make the spectrum doubly degenerate. Under periodic boundary conditions,  $k_x$  and  $k_y$  are good quantum numbers and the energy dispersion for the standard BHZ Hamiltonian supplemented with the BIA term can be calculated to

$$E(k_x, k_y) = \epsilon(k^2) \pm \sqrt{(A|k| \pm h)^2 + M(k^2)^2}. \quad (4)$$

Clearly, the spectrum is non-degenerate for  $|k| \neq 0$ . By additionally introducing the Zeeman terms, the time reversal symmetry is broken and thus the Kramer’s degeneracy at  $|k| = 0$  is lifted.

The combined effect of BIA and Zeeman terms on the bulk energy dispersion is visualized in figure 2 (left). In the following, we choose the Fermi energy  $E_F$  to be zero so that the Fermi level is situated within the gap between the  $E1$ -like bands opened by the Zeeman splitting. The doping parameter is tuned in such a way that  $C \approx -M$ . As a result, only a single pair of Fermi points exists and thus the system has effectively spinless dynamics.

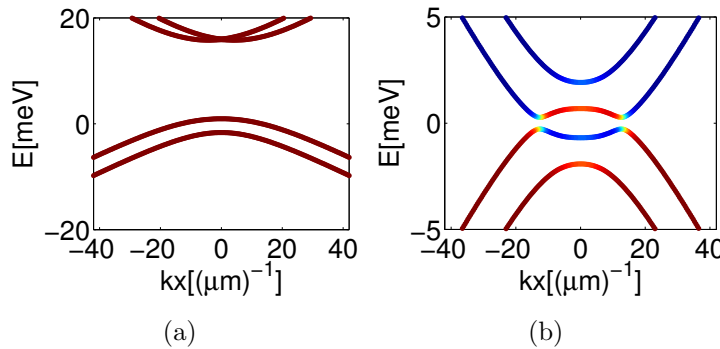


**Figure 2.** Left: Bulk energy dispersion of a HgTe-QW with doping parameter  $C = 7.8 \text{ meV}$  in the presence of Zeeman terms and BIA-SOC; Rashba-SOC is absent and only electron states are shown. Right: The same parameters are used but the s-wave superconducting proximity terms are included. The colors indicate the charge expectation value that ranges between  $e$  (red) and  $-e$  (blue).

When, in addition, the proximity of the s-wave superconductor is taken into account, electrons with energy around the Fermi level and momenta  $k$  and  $-k$  couple,

opening a gap around the Fermi level as shown in figure 2 (right). The special conditions under which this gap closes will be discussed in the following. The Fermi points at which this happens are the key to the emergence of the chiral Majorana edge states [28].

### *Symmetry properties*

Before calculating the Fermi points we will briefly review the symmetry properties of the two  $E1$ -like bands closest to the Fermi level. Their bulk energy spectrum is presented in figure 3 in the presence of different SOC terms: BIA or Rashba or the cooperation of BIA and Rashba. Interestingly, although the spectrum is rotationally symmetric when either Rashba or BIA are present, this rotational symmetry is broken when Rashba and BIA are simultaneously present.

This can be understood as follows [29]: While the effective magnetic fields due to Rashba-SOC are oriented clockwise perpendicular to the wave vector  $k$ , the effective magnetic fields due to BIA spin splitting have a tetrahedral symmetry, as shown in figure 3. When both BIA and Rashba are present, the effective magnetic fields add vectorially, decreasing or enhancing each other. The energy of the lowest-energy band is very sensitive to the effective  $k$ -dependent in-plane magnetic field. Therefore, it exhibits a tetrahedral symmetry when BIA and Rashba interfere with each other.

### *Fermi points*

In the following, we will identify the Fermi points of the spectrum. To simplify analytical calculations, we project the full Hamiltonian (1) onto an effective Hamiltonian. When  $M$  defines the dominant energy scale and the doping is chosen as  $C \approx -M$ , four of the eight bands become irrelevant. Using quasi-degenerate perturbation theory [29] (“Löwdin partitioning”), the eight-band Hamiltonian (1) can be reduced to an effective four-band Hamiltonian acting on the  $E1$ -like electron and hole states only (see Appendix),

$$\begin{aligned} \tilde{H} = & \mu(\hat{k}^2)\tau_z + B_E\sigma_z + \Delta_E\tau_x + R_0\hat{k}_x\sigma_y\tau_z - R_0\hat{k}_y\sigma_x\tau_z \\ & + \tilde{h}\hat{k}_x(\cos 2\theta\sigma_x - \sin 2\theta\sigma_y)\tau_z - \tilde{h}\hat{k}_y(\cos 2\theta\sigma_y + \sin 2\theta\sigma_x)\tau_z. \end{aligned} \quad (5)$$

where the new parameters  $\mu(k^2) = \epsilon(k^2) + M(k^2) + (A^2k^2 + h^2)/(2M)$  and  $\tilde{h} = Ah/M$  have been introduced.

In the absence of BIA-SOC, the reduced form (5) is analogous to the effective Hamiltonians of different semiconductor systems, which have already been shown to host chiral Majorana edge states [8, 30, 10]. Note that the Rashba energy  $U_R \equiv 2m^*R_0^2$  [14] is kept quite small here by intention in order to study the combined effect of BIA and Rashba-SOC: for the values in table 1 it amounts to  $U_R = R_0^2/(\frac{A^2}{2M} - D - B) \approx 0.3$  meV. On the other hand, the BIA-SOC leads to an effective Dresselhaus-SOC in the reduced model (5), which amounts to  $U_D = (Ah/M)^2/(\frac{A^2}{2M} - D - B) \approx 0.7$  meV. In [31], electric fields up to  $\mathcal{E} \sim 100$  mV/nm were estimated to be possible, which could enhance the Rashba energy in principle by a factor of 30, without affecting the effective Dresselhaus energy.

The effective Hamiltonian (5) yields (for  $\theta = \pi/4$  and  $\Delta_E \neq 0$ ) zero energy level crossings at

$$(R_0 - \tilde{h})^2 k_x^2 + (R_0 + \tilde{h})^2 k_y^2 = - \left( |\Delta_E| \pm \sqrt{B_E^2 - \mu(k^2)^2} \right)^2. \quad (6)$$

This implies that for non-vanishing SOC, Fermi points exist (for  $B_E^2 - \mu(k^2)^2 > 0$ ) at

$$k_x = 0, k_y = 0 \text{ and } |\Delta_E| = \sqrt{B_E^2 - \mu_0^2} \quad (7)$$

$$k_x = 0, k_y \neq 0, R_0 = -\tilde{h} \text{ and (6)} \quad (8)$$

$$k_x \neq 0, k_y = 0, R_0 = \tilde{h} \text{ and (6)} \quad (9)$$

where  $\mu_0 = \mu(k^2 = 0) = C + M + h^2/(2M)$ . While the Fermi point (7) exists also in other semiconductor systems that have been proposed to host chiral Majorana edge states [8, 30, 10], the Fermi points (8) and (9) are characteristic of a system with two different SOC terms.

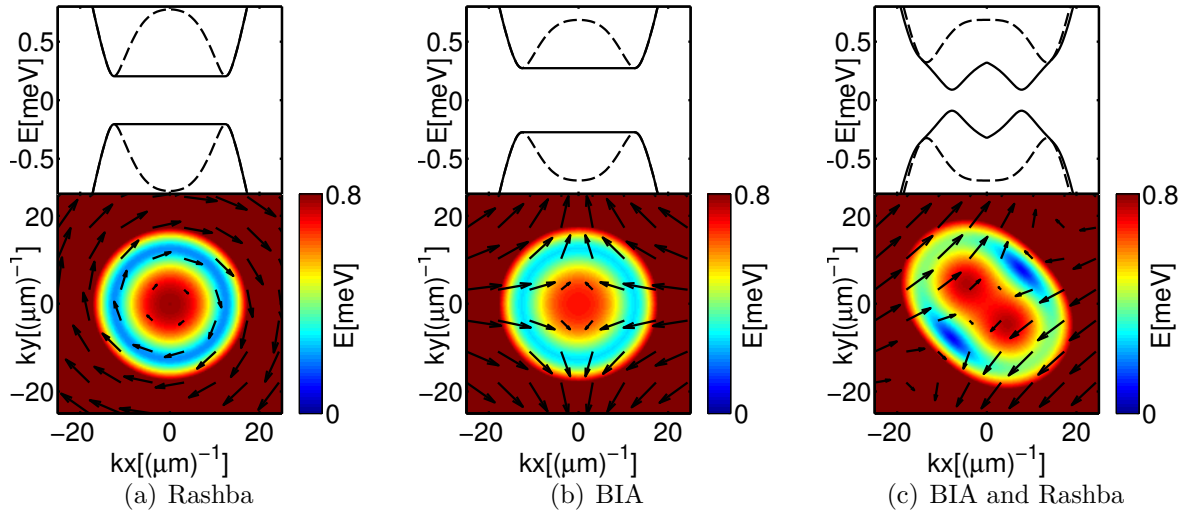


**Figure 3.** Bulk energy dispersion when a) only the Rashba term is included b) only the BIA term is included c) both terms are included. Top: energy dispersion  $E(k_x)$  where  $k_y = 0$  (dashed line) compared to energy dispersion  $E_{min}(k_x)$  where  $k_y$  is such that the energy becomes minimal (solid line). Bottom: energy dispersion  $E(k_x, k_y)$  for the minimal positive energy band. Vectors illustrate in-plane spin expectation values projected onto the E1-band  $\langle \sigma_x(1 + s_z)/2 \rangle$  and  $\langle \sigma_y(1 + s_z)/2 \rangle$ .

### Bulk Topological Invariant

In this section, we identify the topological phases of the non-trivial momentum space topology of Hamiltonian (1). The fundamental Hamiltonian (1) belongs to the Cartan-Altland-Zirnbauer symmetry class  $D$ , which in two spatial dimensions is characterized by a topological invariant  $\in \mathbb{Z}$  [32]. The first Chern number which is commonly used as the topological invariant can be obtained for a non-interacting Hamiltonian with

non-degenerate spectrum as the integral of the Berry curvature over the first Brillouin zone

$$\mathcal{C}_1 = \frac{1}{2\pi} \int_{\text{BZ}} \mathcal{F} d^2k \quad (10)$$

where the Berry curvature  $\mathcal{F} = \partial_{k_x} \mathcal{A}_{k_y} - \partial_{k_y} \mathcal{A}_{k_x}$  is obtained from the Bloch functions via  $\mathcal{A}_{k_\alpha} = -i \sum_j \langle u_j(k) | \partial_{k_\alpha} | u_j(k) \rangle$ ,  $\alpha = x, y$ , the index  $j$  running over the occupied states.

For non-vanishing spin-orbit interactions<sup>+</sup>, the first Chern number of the Hamiltonian (1) is given by

$$\mathcal{C}_1 = \Theta(B_E^2 - \mu_0^2 - \Delta_E^2) \text{sign}(R_0^2 - \tilde{h}^2), \quad (11)$$

where  $\Theta(x)$  is the Heaviside step function. This was verified by computing the topological invariant from a discretized version [33] of (10) for a regularized version\* of Hamiltonian (1) numerically using MATLAB at several illustrative values of the parameters on each side of the topological transitions. Equation (11) is valid when the BIA parameter  $h$  is small compared to the mass parameter  $M$ .

While the general form of (11) is analogous to known topological invariants of similar systems such as spin-orbit coupled quantum wires [10] or 2D spin-orbit coupled semiconductors [8], this constitutes to our knowledge the first such calculation for a HgTe-QW in proximity to a superconductor. Importantly, this is also the first time that the BIA term  $h$  is included. When both Rashba and BIA are present, the sign of the topological invariant  $\mathcal{C}_1$  can be reversed due to the interplay between both SOC's. This is similar to the combined effect of Rashba and Dresselhaus SOC's that was described for non-centrosymmetric superconductors [34].

In the absence of BIA, the relevant parameters for a topological transition to occur are the proximity coupling  $\Delta_E$ , the Zeeman energy  $B_E$  and the sum of mass gap and doping,  $\mu_0 = C + M$ . When BIA is taken into account, the topological transition is shifted towards higher doping as described by the term  $\mu_0 = C + M + \frac{h^2}{2M}$  (in the limit that  $M$  is the dominant energy scale). The topological transition is presented as a function of Zeeman energy  $B_E$  and doping  $C$  in figure 4.

#### 4. Majorana Edge States

In this section, we discuss the appearance of Majorana edge states in this system.

With an edge we mean that there is a domain wall in the shape of a straight edge where one side is topologically nontrivial ( $\mathcal{C}_1 = \pm 1$ ) and the other side is topologically trivial ( $\mathcal{C}_1 = 0$ ). We distinguish between two cases: either (i) the topologically nontrivial region is vacuum or (ii) a topologically trivial QW. In the following, these cases will be referred as (i) hard-wall boundary conditions and (ii) soft-wall boundary conditions. Soft-wall

<sup>+</sup> i.e. BIA and Rashba should not both be zero

<sup>\*</sup> i.e. replacing  $k_x^2 + k_y^2 \rightarrow \frac{2}{a^2} (2 - \cos(ak_x) - \cos(ak_y))$ ,  $k_x \rightarrow \frac{1}{a} \sin(ak_x)$ ,  $k_y \rightarrow \frac{1}{a} \sin(ak_y)$  where  $a$  is a lattice constant that is chosen in such a way that no artificial level crossings occur.



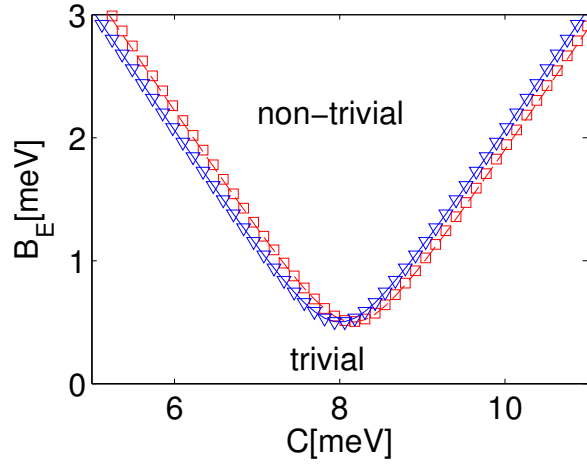


**Figure 4.** Topological phase diagram in the parameter region Zeeman energy  $B_E$  and doping  $C$ . The topological transition described approximatively by (11) (blue solid line when BIA is present, red dashed line when BIA is absent) is compared to numerical calculations based on (1) (blue triangle when BIA is present, red square when BIA is absent). When BIA asymmetry is taken into account, the topological transition is shifted towards higher doping. The other parameters are given in table 1.

boundary conditions (two different topological phases in a QW) can be achieved by varying the doping parameter  $C$  accordingly across the sample, as shown in figure 5 (b).

Without loss of generality, we assume that the domain wall lies parallel to the  $x$ -axis and that the region  $y < 0$  is topologically non-trivial while  $y > 0$  is topologically trivial. Due to translational invariance along the  $x$ -axis we can consider solutions that propagate along the edge with definite  $k_x$ .

The general strategy when solving such a boundary problem is as follows: In a first step, we use the Ansatz

$$\psi(x, y, E) = e^{ik_x x} e^{ik_y y} \psi(k_x, k_y), \quad (12)$$

to calculate the wave functions on both sides of the boundary. Hereby,  $k_y$ , which is not a good quantum number, has to be determined as a function of  $k_x$  and the energy  $E$  separately for both sides of the boundary. In addition, the eigenvectors are determined as a function of  $k_x$  and  $E$ .

In the second step, the boundary conditions are applied, finally yielding an energy dispersion  $E(k_x)$ . For hard wall boundary conditions, the wave function is required to vanish at the boundary between the HgTe sample and vacuum. For soft wall boundary conditions, both the wave function and its first derivative are required to be continuous at the boundary between the topologically trivial and the topologically non-trivial HgTe samples. In both cases, we require that the solutions are bound to the edge, i.e. that the probability densities vanish far away from the boundary (see figure 5).

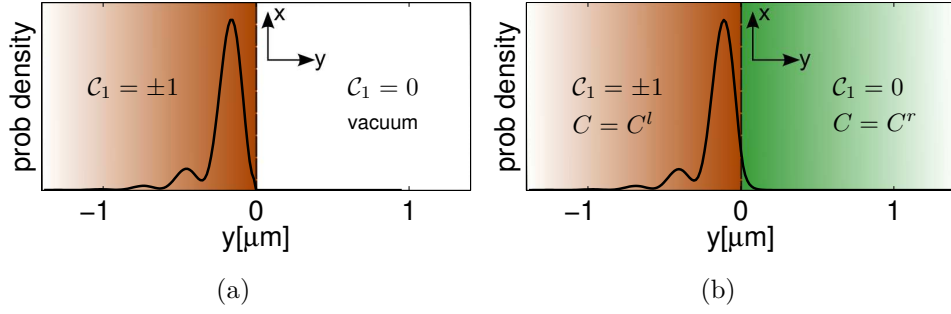


**Figure 5.** Normalized probability density at  $k_x = 0$  as a function of  $y$  for soft wall boundary conditions separating a topologically non-trivial QW from vacuum (trivial) (a) and hard wall boundary conditions separating a topologically non-trivial QW region from a topologically trivial QW region.

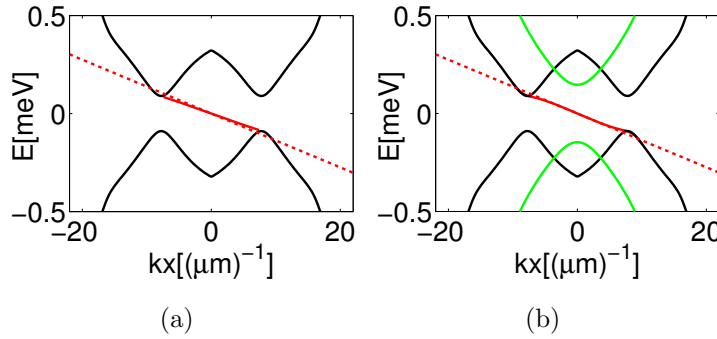


**Figure 6.** Energy dispersion with a boundary in  $x$ -direction. On the left hand side of the boundary there is a topologically non-trivial QW with  $C^l = 7.8$  meV (black bulk energy minimum), while on the right hand side of the boundary there is either vacuum (a) or a topologically trivial QW with  $C^r = 6.8$  meV, indicated by the green bulk energy minimum (b). Chiral Majorana edge states obtained numerically as boundary solutions to (1) are shown in red. The red dotted lines are estimations derived from (17). The parameter values are taken from table 1.

### Calculation of edge state dispersion for small $k_x$

Under certain simplifying assumptions, the edge dispersion of the boundary problem can be calculated to first order in  $k$  using perturbation theory. We assume that is sufficient to calculate the edge dispersion in the reduced model (5) and require that quadratic terms  $\propto k_x^2, k_y^2$  may be neglected (Assumption 1). Consistently, we also match only the wave functions and not the derivatives at the boundary.

We first prove that the boundary conditions are fulfilled for  $E = 0, k_x = 0$  and calculate the wave function of the corresponding bound state.

Imposing the condition  $E = k_x = 0$  in (5) yields four possible values for  $\lambda = ik_y$ :

$$\pm \lambda_{\pm} = \frac{\pm \left( |\Delta_E| \pm \sqrt{B_E^2 - \mu_0^2} \right)}{\sqrt{R_0^2 + \tilde{h}^2 + 2R_0\tilde{h} \sin 2\theta}}. \quad (13)$$

Depending on the parameter values, the signs of  $\lambda$  can be determined as follows under

the assumption that  $|B_E| > |\mu_0|$ :

$$\begin{array}{c|c} B_E^2 > \mu_0^2 + \Delta_E^2 & B_E^2 < \mu_0^2 + \Delta_E^2 \\ \hline +\lambda_+ > 0 & +\lambda_+ > 0 \\ -\lambda_- > 0 & +\lambda_- > 0 \end{array}$$

The respective eigenvectors are

$$|\lambda_+\rangle = \frac{1}{2} \begin{pmatrix} e^{i\chi} \sqrt{1 - \mu_0/B_E} \\ -\text{sign}(B_E) \sqrt{1 + \mu_0/B_E} \\ e^{i\chi} \text{sign}(B_E) \sqrt{1 + \mu_0/B_E} \\ \sqrt{1 - \mu_0/B_E} \end{pmatrix} \quad (14)$$

with  $e^{i\chi} = (iR_0 + \tilde{h}e^{2\theta i}) / \sqrt{R_0^2 + \tilde{h}^2 + 2R_0\tilde{h}\sin 2\theta}$  and where  $|\lambda_- \rangle$ ,  $|\lambda_+ \rangle$  and  $|\lambda_- \rangle$  can be obtained from  $|\lambda_+ \rangle$  by clockwise translation of the minus sign in front of the second entry.

If  $B_E^2 > \mu_l^2 + \Delta_E^2$  on the left side of the boundary (topologically non-trivial) and  $B_E^2 < \mu_r^2 + \Delta_E^2$  on the right side of the boundary (topologically trivial), the matching condition requires that the eigenvectors on the left and right hand sides of the boundary are linearly dependent,

$$\det(|\lambda_+^l\rangle, |\lambda_-^l\rangle, |\lambda_+^r\rangle, |\lambda_-^r\rangle) = 0 \quad (15)$$

yielding the solution

$$\psi(y) = \frac{1}{\mathcal{N}} \left( \Theta(-y) e^{-\lambda_-^l y} |\lambda_-^l\rangle + \Theta(y) (c_1 e^{-\lambda_+^r y} |\lambda_+^r\rangle + c_2 e^{-\lambda_-^r y} |\lambda_-^r\rangle) \right). \quad (16)$$

Here  $\mathcal{N}$  is a normalization factor such that  $\int dy |\psi(y)|^2 = 1$ . The coefficients  $c_1$  and  $c_2$  are determined by the matching condition.

This proves that there is a bound state for  $k_x = E = 0$ . The antisymmetry of the Hamiltonian (1) under particle-hole transformation  $\Xi^\dagger H \Xi = -H$ , where  $\Xi = iK\sigma_y\tau_y$ , has the important consequence that  $\psi(y)$  for  $k_x = E = 0$  constitutes a Majorana excitation, as can be easily confirmed by explicit calculation.

Now we consider the case of non-zero  $k_x$ . When  $k_x$  is small, the  $k_x$ -dependent BIA and Rashba terms in equation (5) can be treated as a perturbation  $V$ . The expectation value of this perturbation with respect to the  $k_x = E = 0$  state gives the energy in terms of  $k_x$  to first order in perturbation theory,

$$E = \int dy \psi^*(y) V \psi(y) = \frac{|\Delta_E|}{B_E} \frac{R_0^2 - \frac{A^2 h^2}{M^2}}{\sqrt{R_0^2 + \frac{A^2 h^2}{M^2} + 2R_0 \frac{Ah}{M} \sin 2\theta}} k_x. \quad (17)$$

### Edge state dispersions

The resulting edge energy dispersions that were calculated numerically from (1) and using (17) are presented and compared to the bulk energy dispersions in figure 6.

The boundary between topologically trivial and non-trivial regions results in a single chiral Majorana bound state of approximately linear energy dispersion that smoothly

connects to the occupied and non-occupied bulk bands. The existence of this edge state is independent of which boundary condition (soft or hard wall) or which inversion asymmetry term (BIA, Rashba or both) is considered. As expected, its existence depends on the topological bulk properties on both sides of the boundary - the edge state disappears when the Chern numbers on both sides of the boundary are identical.

The formula (17) describes the numerically obtained energy dispersions of figure 6 well, regardless of whether hard wall or soft wall boundary conditions have been employed. A small discrepancy between the numerical calculation on the basis of the Hamiltonian (1) and (17) is mostly due to the limited applicability of Assumption 1. Yet, (17) describes the salient features of the edge dispersion well.

As predicted by (17), the edge state velocity depends most strongly on the parameters  $\theta, A, h, R_0, B_E, \Delta_E$ . We have checked that the parameters  $D, B, C, \Delta_H, B_H$  have comparably little effect on the energy dispersion.

Interestingly, we find that the group velocity  $v = \frac{1}{\hbar} \frac{\partial E}{\partial k_x}$  of the chiral edge state is tunable by the interplay between the Rashba and BIA spin-orbit interactions. The edge state is right-moving when the Rashba term dominates and left-moving when the BIA term dominates (see figure 7). This is consistent with the change of the first Chern number in (11) between  $\mathcal{C}_1 = \pm 1$  by means of the index theorem [28]. When applied to the hard-wall boundary condition, the index theorem equates the topological charge  $\mathcal{C}_1$  of the bulk with the sign  $\nu$  of the slope of the chiral edge mode. It is therefore easy to see that as the Rashba parameter  $R_0$  changes from  $R_0^2 < \tilde{h}^2$  to  $R_0^2 > \tilde{h}^2$ , the first Chern number changes from  $-1$  to  $+1$  and the edge state from left to right moving. This could be experimentally verified by changing the Rashba parameter, while the intrinsic BIA-SOC remains fixed. Another interesting observation is that the group velocity of the chiral Majorana edge state depends on the orientation of the edge with respect to the crystal axis when both Rashba and BIA SOC terms are present. The absolute values of the velocity is smallest along the  $[110]$  ( $\theta = \pi/4$ ) and largest along the  $[\bar{1}10]$  ( $\theta = 3\pi/4$ ) direction. In HgTe-QWs, the edge structures are for experimental reasons prepared in parallel to the cleavage planes, and therefore 95 % of the current carrying edges are orientated either in  $[110]$  or  $[\bar{1}10]$  direction [35]. Due to the simultaneous presence of Rashba and BIA SOC terms, these two experimentally accessible edge orientations are expected to have distinct chiral Majorana edge state properties.

## 5. Comparison of chiral Majorana edge states and helical edge states

As described in the previous section, a HgTe-QW in proximity to a superconductor with BIA and a Zeeman field hosts chiral Majorana edge states at its edges when the parameters are in the topological nontrivial TSC phase ( $\mathcal{C}_1 = \pm 1$ ).

On the other hand, it is well-known that a time-reversal invariant HgTe-QW hosts helical edge states at its boundary [16, 19, 36] when the mass parameter  $M$  is negative ( $B/M > 0$ ).

In the following, we will compare the chiral Majorana edge states and the helical

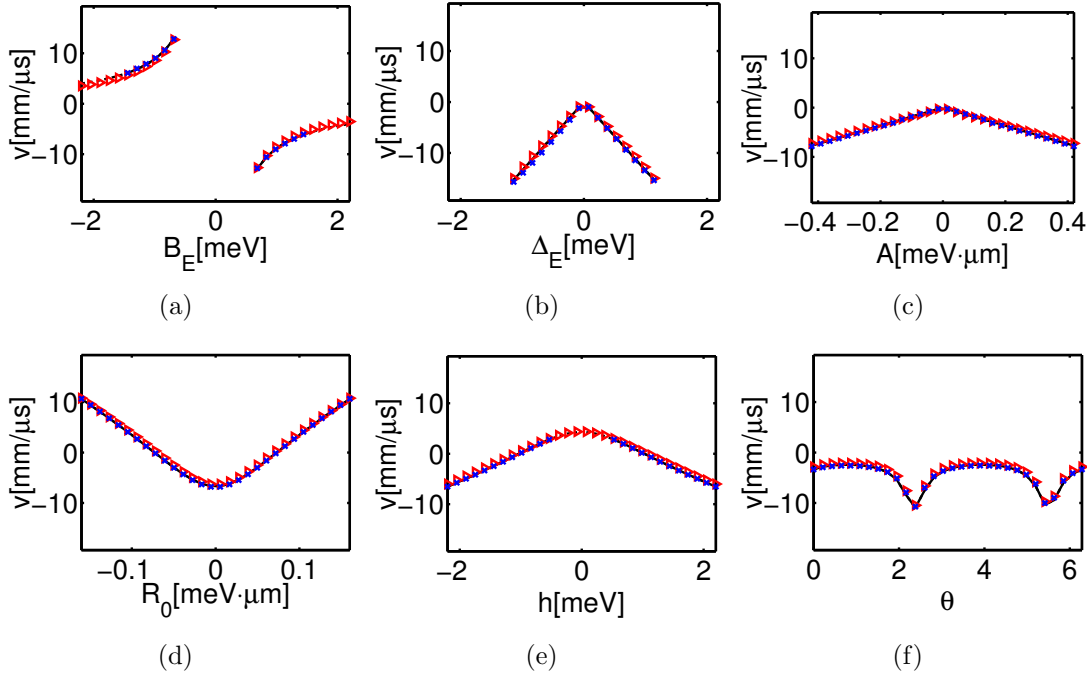


**Figure 7.** The edge group velocities  $v = \frac{1}{\hbar} \frac{\partial E}{\partial k_x}$  as a function of different parameters. Analytic approximations (solid black lines) obtained from (17) are compared with numerical values for hard wall (red triangles) and soft wall boundary conditions (blue crosses). This confirms that the edge state only exists when the boundary connects topologically trivial and non-trivial regions, compare (11). The Rashba spin-orbit coupling is set to zero except in the last line; all other parameters are taken from table 1.

(Dirac) edge states, assuming that only the BIA-SOC term is present.

Chiral Majorana edge states and helical edge states at a single boundary are mutually exclusive. Firstly, helical edge states are not topologically protected when time reversal symmetry is broken by an Zeeman field, which is needed for the emergence of chiral Majorana edge states [36]. Secondly, it has recently been shown that even in the presence of time reversal symmetry, the introduction of the superconducting term  $\Delta\tau_x$  adiabatically interconnects the regions that in its absence would differ by their topological invariants [37].

In the parameter range where there is a chiral Majorana edge state, there are therefore no additional helical edge states within the bulk energy gap, see figure 8 (a,b). Even if the mass gap  $M$  is negative, potential helical edge states are gapped out by the proximity of the superconductor.

For comparison to the chiral Majorana edge states, the helical edge states are shown in the absence of both the Zeeman field and the superconductor in figure 8 (c,d), where in contrast to the standard HgTe the additional BIA term is included. As reported in [38], it has a negligible effect, and the velocity of the helical edge states is still well-described by [39]

$$E = -\frac{D}{B}M \pm k_x A \sqrt{\frac{B^2 - D^2}{B^2}} \quad (18)$$

for small  $|k_x|$ . The chiral and helical edge states differ greatly in their velocities, which are given by (17) and (18), respectively. The offset is also different: While chiral Majorana edge states are confined to the crossing  $k_x = E = 0$  by particle hole symmetry, the helical edge states are only restricted to crossing each other somewhere on the  $E$  axis by time reversal symmetry.

Helical and chiral edge states have similar widths. While recent calculations for the width of helical edge states predict an edge width under 100 nm in a HgTe-QW near the Dirac point [39], experimentally confirmed up to a factor of 2 in [40], the chiral Majorana edge states typically extend to about 200 nm-300 nm in a HgTe-QW for the parameters in table 1.

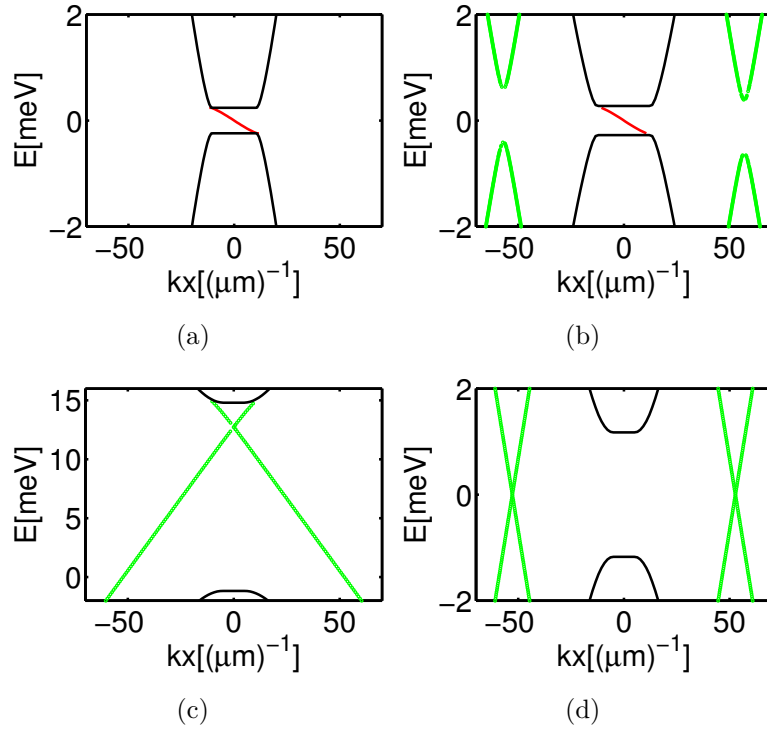


**Figure 8.** Energy dispersion with a hard wall boundary in  $x$ -direction for a HgTe-QW with topologically nontrivial parameters (a)  $C = -7.8$  meV,  $M = 8$  meV and (b)  $C = 7.8$  meV,  $M = -8$  meV. This allows chiral Majorana edge states to form. All other parameters except the Rashba-SOC, which is set to zero, are taken from table 1. In (c,d), the energy dispersions of a time-reversal invariant HgTe-QW in the inverted regime without the presence of the superconductor are shown ( $C = 6.8$  meV,  $M = -8$  meV). For better comparison with (b), the degrees of freedom have been doubled in (d) by reflection at the Fermi level.

### Summary

In summary, we have shown that a HgTe/CdTe QW in the proximity to an s-wave superconductor and the presence of a Zeeman-splitting can represent a TSC with chiral one-dimensional edge states. At  $k_x=E=0$ , these quasiparticles have the Majorana

property of being their own antiparticle.

Importantly, an external electric field that leads to an additional Rashba-SOC term is not required, as long as the intrinsic BIA is large enough. While in most publications, BIA is discussed as an unwanted but small perturbation, in this case a high BIA would be of interest. Interestingly, if Rashba-SOC and BIA-SOC are both present, the group velocity  $v = \frac{1}{\hbar} \frac{\partial E}{\partial k_x}$  of the chiral edge state depends crucially on the interplay between both spin-orbit interactions and can be reversed if the Rashba-SOC is tuned from zero to a value that exceeds the bulk inversion asymmetry term. We discussed in analytical and numerical terms in which parameter regime the TSC exists using the extended four-band model of BHZ valid near the topological phase transition between a trivial and a non-trivial TI that would exist without the superconducting and Zeeman terms.

Although many systems hosting chiral Majorana fermions have so far been presented [5, 10], this is the first proposal to switch between one-dimensional Majorana- and Dirac edge states in a (HgTe) QW, rather than the surface of a 3D TI, where different scenarios to convert between one-dimensional Majorana- and Dirac edge states have previously been proposed [41, 42, 43], and the first time chiral Majorana- and helical Dirac edge states appear in the same system.

The possibility to switch between chiral Majorana- and helical Dirac edge states on the same one-dimensional boundary might not only enhance experimental control in the detection of Majorana quasiparticles, but could also provide an interesting framework that combines dissipationless transport and the non-local storage of quantum information.

Importantly, we would like to point out that our analysis should equally well hold for other 2D TIs, like type-II QWs made of InAs/GaSb/AlSb, which have intrinsically inverted bandstructures and similar inversion symmetry breaking SOC terms [44]. Experimental evidence of the quantum spin Hall effect in these systems has recently been given [45], also in connection with superconducting contacts [46]. Further, it has been proposed that bilayer HgTe-based QWs in the presence of an interlayer voltage allows for an all electrically tunable TI [47, 48].

### *Acknowledgments*

We would like to thank Hartmut Buhmann for enlightening discussions, Jan Budich and Björn Trauzettel for useful comments on the manuscript and financial support from the "NTH school for contacts in nanosystems" and the DFG grant RE 2978/1-1.

## Appendix

If the mass gap  $M$  is the relevant energy scale of the problem, leading to only four relevant  $E1$ -like energy bands, this allows us to reduce the eight-band Hamiltonian (1) onto an effective four-band Hamiltonian.

To this end, we divide the Hamiltonian into three parts,

$$H = H_0 + H_1 + H_2 \quad (\text{A.1})$$

$$H_0 = (C + Ms_z) \tau_z \quad (\text{A.2})$$

$$H_1 = R_0 \frac{(s_z + 1)}{2} (\hat{k}_x \sigma_y - \hat{k}_y \sigma_x) \tau_z \quad (\text{A.3})$$

$$+ (\Delta_+ + \Delta_- s_z) \tau_x - (B + D) \hat{k}^2 + (B_+ + B_- s_z) \sigma_z$$

$$H_2 = A \hat{k}_x s_x \sigma_z \tau_z - A \hat{k}_y s_y \tau_z + h \sigma_y s_y \tau_z. \quad (\text{A.4})$$

where for clarity, in contrast to the more general Hamiltonian (1), we set  $\theta = 0$ .

In the following,  $H_0$  (containing only  $s_z$ ) is considered as the unperturbed Hamiltonian and  $H_1$  (containing only  $s_z$ ) and  $H_2$  (containing  $s_y$ ) as the block-diagonal and block-offdiagonal perturbations, respectively. The perturbations are small in the sense that the mass gap  $M$  is the dominant energy scale, i.e.

$$|\Delta_\pm|, |B_\pm|, |h|, |A||k|, |R_0||k|, |B||k|^2, |D||k|^2 \ll |M| \quad (\text{A.5})$$

In order to approximately diagonalize the Hamiltonian  $H$ ,

$$\tilde{H} = e^{-S} H e^S \quad (\text{A.6})$$

we apply quasi-degenerate perturbation theory (“Löwdin partitioning”) [29].

The important matrix for the transformation,  $S$ , consists of different orders of the perturbation parameter,  $S = S^{(1)} + \mathcal{O}(2)$ . It can be shown that

$$\tilde{H} = H_0 + H_1 + \frac{1}{2} [H_2, S^{(1)}] + \mathcal{O}(3) \quad (\text{A.7})$$

is block-diagonal up to second order if  $S^{(1)}$  is determined in such a way that

$$[H_0, S^{(1)}] = -H_2. \quad (\text{A.8})$$

For the Hamiltonian (A.1) it is straight-forward to show $\sharp$  that

$$S^{(1)} = +i \frac{h}{2M} s_x \sigma_y - i \frac{A \hat{k}_x}{2M} s_y \sigma_z - i \frac{A \hat{k}_y}{2M} s_x \quad (\text{A.9})$$

$$\begin{aligned} \tilde{H} = & \mu(s_z, \hat{k}) \tau_z + B(s_z) \sigma_z + \Delta(s_z) \tau_x \\ & + \tilde{h} \hat{k}_x \sigma_x \tau_z - \tilde{h} \hat{k}_y s_z \sigma_y \tau_z + R(s_z) \hat{k}_x \sigma_y \tau_z - R(s_z) \hat{k}_y \sigma_x \tau_z \end{aligned} \quad (\text{A.10})$$

where the new parameters

$$\mu(s_z, \hat{k}^2) = \epsilon(\hat{k}_y) + \left( M(\hat{k}^2) + \frac{A^2 \hat{k}^2}{2M} + \frac{h^2}{2M} \right) s_z \quad (\text{A.11})$$

$\sharp$  under the requirement that the parameters do not depend on  $x$  or  $y$ .



$$B(s_z) = B_+ + B_- s_z \quad (\text{A.12})$$

$$\Delta(s_z) = \Delta_+ + \Delta_- s_z \quad (\text{A.13})$$

$$\tilde{h} = \frac{Ah}{M} \quad (\text{A.14})$$

$$R(s_z) = R_0 \frac{(s_z + 1)}{2} \quad (\text{A.15})$$

have been introduced. The advantage of the transformed Hamiltonian (A.10) is that  $s_z$  is (approximately) a good quantum number. For further calculations, we neglect the  $s_z = -1$  solutions in the main text (5), and retrieve the angular dependence on  $\theta$  by the simple replacement rules

$$h\sigma_y \rightarrow h(\cos 2\theta\sigma_y + \sin 2\theta\sigma_x) \quad (\text{A.16})$$

$$h\sigma_x \rightarrow h(\cos 2\theta\sigma_x - \sin 2\theta\sigma_y) \quad (\text{A.17})$$

which amount to a rotation in the  $xy$ -plane.

- [1] M. Z. Hasan and C. L. Kane, Rev. Mod. Phys. **82**, 3045 (2010).
- [2] X.-L. Qi and S.-C. Zhang, Rev. Mod. Phys. **83**, 1057 (2011).
- [3] J. Alicea, Rep. Prog. Phys. **75**, 076501 (2012).
- [4] C. W. J. Beenakker, arXiv:1112.1950 (2011).
- [5] L. Fu and C. L. Kane, Phys. Rev. Lett. **100**, 096407 (2008).
- [6] L. Fu and C. L. Kane, Phys. Rev. B **79**, 161408 (2009).
- [7] J. Nilsson, A. R. Akhmerov, and C. W. J. Beenakker, Phys. Rev. Lett. **101**, 120403 (2008).
- [8] J. D. Sau, R. M. Lutchyn, S. Tewari, and S. Das Sarma, Phys. Rev. Lett. **104**, 040502 (2010).
- [9] J. Alicea, Phys. Rev. B **81**, 125318 (2010).
- [10] Y. Oreg, G. Refael, and F. von Oppen, Phys. Rev. Lett. **105**, 177002 (2010).
- [11] V. Mourik *et al.*, Science **336**, 1003 (2012).
- [12] M. T. Deng *et al.*, Nano Lett. **12**, 6414 (2012).
- [13] A. Das *et al.*, Nature Phys. **8**, 887 (2012).
- [14] A. C. Potter and P. A. Lee, Phys. Rev. B **83**, 184520 (2011).
- [15] J. D. Sau, S. Tewari, and S. Das Sarma, Phys. Rev. B **85**, 064512 (2012).
- [16] B. A. Bernevig, T. L. Hughes, and S.-C. Zhang, Science **314**, 1757 (2006).
- [17] D. G. Rothe *et al.*, New J. Phys. **12**, 065012 (2010).
- [18] M. König, H. Buhmann, L. W. Molenkamp, and T. Hughes, J. Phys. Soc. Japan **77**, 031007 (2008).
- [19] M. König *et al.*, Science **318**, 766 (2007).
- [20] A. Roth *et al.*, Science **325**, 294 (2009).
- [21] R. Winkler, L. Wang, Y. Lin, and C. Chu, Solid State Commun. **152**, 2096 (2012).
- [22] Y. S. Gui *et al.*, Phys. Rev. B **70**, 115328 (2004).
- [23] J. P. Heida *et al.*, Phys. Rev. B **57**, 11911 (1998).
- [24] B. Büttner *et al.*, Nature Phys. **7**, 418 (2011).
- [25] C.-X. Liu *et al.*, Phys. Rev. Lett. **101**, 146802 (2008).
- [26] M. Guigou and J. Cayssol, Phys. Rev. B **82**, 115312 (2010).
- [27] G. Tkachov *et al.*, Phys. Rev. Lett. **106**, 076802 (2011).
- [28] G. E. Volovik, *The Universe in a Helium Droplet* (Oxford University Press, Oxford, 2003).
- [29] R. Winkler, *Spin-orbit coupling effects in two-dimensional electron and hole systems*, No. 191 in *Springer tracts in modern physics* (Springer, Berlin ; Heidelberg [u.a.], 2003).
- [30] P. Ghosh, J. D. Sau, S. Tewari, and S. Das Sarma, Phys. Rev. B **82**, 184525 (2010).
- [31] P. Virtanen and P. Recher, Phys. Rev. B **85**, 035310 (2012).
- [32] A. Altland and M. R. Zirnbauer, Phys. Rev. B **55**, 1142 (1997).
- [33] R. Resta (unpublished).
- [34] J. You, C. H. Oh, and V. Vedral, arXiv:1209.0930 (2012).
- [35] Private communications with H. Buhmann.
- [36] X.-L. Qi, T. L. Hughes, and S.-C. Zhang, Phys. Rev. B **78**, 195424 (2008).
- [37] J. C. Budich, arXiv:1301.5339 (2013).
- [38] P. Michetti, P. H. Penteado, J. C. Egues, and P. Recher, Semicond. Sci. Tech. **27**, 124007 (2012).
- [39] B. Zhou *et al.*, Phys. Rev. Lett. **101**, 246807 (2008).
- [40] Y. Ma *et al.*, arXiv:1212.6441 (2012).
- [41] L. Fu and C. L. Kane, Phys. Rev. Lett. **102**, 216403 (2009).
- [42] A. R. Akhmerov, J. Nilsson, and C. W. J. Beenakker, Phys. Rev. Lett. **102**, 216404 (2009).
- [43] C.-X. Liu and B. Trauzettel, Phys. Rev. B **83**, 220510 (2011).
- [44] C. Liu *et al.*, Phys. Rev. Lett. **100**, 236601 (2008).
- [45] I. Knez, R.-R. Du, and G. Sullivan, Phys. Rev. Lett. **107**, 136603 (2011).
- [46] I. Knez, R.-R. Du, and G. Sullivan, Phys. Rev. Lett. **109**, 186603 (2012).
- [47] P. Michetti, J. C. Budich, E. G. Novik, and P. Recher, Phys. Rev. B **85**, 125309 (2012).
- [48] P. Michetti and B. Trauzettel, arXiv:1301.1823 (2013).